

Highlights

PEFT-MuTS: A Multivariate Parameter-Efficient Fine-Tuning Framework for Remaining Useful Life Prediction based on Cross-domain Time Series Representation Model

En Fu, Yanyan Hu, Changhua Hu, Zengwang Jin, Kaixiang Peng

- Cross-domain time-series priors enable accurate few-shot RUL prediction.
- PEFT-MuTS efficiently adapts pretrained model to multivariate RUL prediction.
- A 0-initialized regressor is proposed to stabilize fine-tuning in RUL prediction.

PEFT-MuTS: A Multivariate Parameter-Efficient Fine-Tuning Framework for Remaining Useful Life Prediction based on Cross-domain Time Series Representation Model[★]

En Fu^a, Yanyan Hu^{b,c,*}, Changhua Hu^d, Zengwang Jin^e and Kaixiang Peng^{b,c}

^aSchool of Intelligence Science and Technology, University of Science and Technology Beijing, Beijing, 100083, Beijing, China

^bSchool of Automation and Electrical Engineering, University of Science and Technology Beijing, Beijing, 100083, Beijing, China

^cKey Laboratory of Knowledge Automation for Industrial Processes of the Ministry of Education, University of Science and Technology Beijing, Beijing, 100083, Beijing, China

^dRocket Force University of Engineering, Xi'an, 710000, Shaanxi, China

^eInstitute of Embodied Intelligence, Anhui University, Hefei, 230601, Anhui, China

ARTICLE INFO

Keywords:

Remaining Useful Life
Transfer Learning
Parameter-Efficient Fine-Tuning
Few-shot Learning

ABSTRACT

The application of data-driven remaining useful life (RUL) prediction has long been constrained by the availability of large amount of degradation data. Mainstream solutions such as domain adaptation and meta-learning still rely on large amounts of historical degradation data from equipment that is identical or similar to the target, which imposes significant limitations in practical applications. This study investigates PEFT-MuTS, a Parameter-Efficient Fine-Tuning framework for few-shot RUL prediction, built on cross-domain pre-trained time-series representation models. Contrary to the widely held view that knowledge transfer in RUL prediction can only occur within similar devices, we demonstrate that substantial benefits can be achieved through pre-training process with large-scale cross-domain time series datasets. A independent feature tuning network and a meta-variable-based low rank multivariate fusion mechanism are developed to enable the pre-trained univariate time-series representation backbone model to fully exploit the multivariate relationships in degradation data for downstream RUL prediction task. Additionally, we introduce a zero-initialized regressor that stabilizes the fine-tuning process under few-shot conditions. Experiments on aero-engine and industrial bearing datasets demonstrate that our method can achieve effective RUL prediction even when less than 1% of samples of target equipment are used. Meanwhile, it substantially outperforms conventional supervised and few-shot approaches while markedly reducing the data required to achieve high predictive accuracy. Our code is available at <https://github.com/fuen1590/PEFT-MuTS>.

1. Introduction

Remaining Useful Life (RUL) prediction aims to quantitatively estimates the remaining effective time of equipment, providing objective basis for maintenance decisions or replacement plans[1, 2, 3]. As a key means of avoiding maintenance surplus and deficiency, RUL prediction constitutes the core function of the new generation of Prognostics and Health Management (PHM)[4]. In recent years, deep-learning based RUL prediction methods have attracted increasing attention for their ability to establish accurate end-to-end mapping between monitoring signals and the RUL label without reliance on any expert knowledge. What these methods primarily rely on is a substantial amount of full-lifecycle degradation data for sufficient model training. However, collecting such run-to-failure full-lifecycle data in real industrial settings is always costly and challenging, which significantly hinders the practical adoption of deep-learning based RUL prediction methods.

To solve the RUL prediction problem under few-shot domains, transfer learning, represented by domain adaptation[5, 6, 7, 8, 9, 10, 11] and meta-learning[12, 13, 14, 15, 16, 17], has becoming as a mainstream approach.

[★]This work is supported by the National Natural Science Foundation of China (Grant 62273038), the Open Fund of Intelligent Control Laboratory (Grant 2024-ZKSYS-KF03-05) and the Ningbo Young Technological Innovation Leading Talent Project of China (Grant 2025QL047)

*Corresponding author

 fuen@xs.ustb.edu.cn (E. Fu); huyanyan@ustb.edu.cn (Y. Hu); hch-reu@mail.nwpu.edu.cn (C. Hu);
Jin_zengwang@nwpu.edu.cn (Z. Jin); kaixiang@ustb.edu.cn (K. Peng)

ORCID(s): 0009-0006-4837-6711 (E. Fu); 0000-0003-3578-7598 (Y. Hu); 0000-0002-7491-9103 (Z. Jin); 0000-0001-8314-3047 (K. Peng)

The core idea of transfer learning is to leverage the prior knowledge of source domain to target domain by constructing an effective transfer pathway. Although extensive transfer learning-based methods have been developed for few-shot RUL prediction, the majority are limited to transfer across different operating conditions of similar equipment. In other words, the focus of existing methods is on identifying consistent degradation pattern of similar devices under distinct operation conditions. Thus, a prerequisite of these methods is sufficient degradation data from similar equipment can be available to construct the source domain for transfer, which is still a stringent requirement in many practical applications. When historical data of the target equipment is scarce, it may be equally difficult to collect a substantial amount of data from similar equipment. For example, the operational lifespan of many types of industrial assets extends for decades, making full lifecycle data collection a long process and time-consuming. Another example is the newly developed or small batch customized equipment domain. The historical degradation data of such kinds of equipment is considerably limited due to the short service time and small quantity. To sum up, existing few-shot RUL prediction methods based on the idea of device-specific degradation pattern transfer will become infeasible when sufficient degradation data with similar degradation pattern from homogeneous equipment cannot be obtained, which significantly undermines their values in practical application.

As we known, degradation data for RUL prediction are predominantly time series data, thereby recent advances in time-series representation learning offer a promising way to overcome above limitations. Time series representation models trained in a self-supervised manner can learn generalizable temporal feature representations from large-scale time series datasets. It has been proved that the pre-trained time series representation models have strong generalization ability in cross-domain downstream classification and prediction tasks[18, 19, 20]. Consequently, leveraging the excellent generalization ability of time series representation model to RUL prediction has the potential to significantly improving the accuracy and robustness of prediction result, especially in few-shot scenes. Moreover, the pre-training process of representation model is not tied to a specific downstream task. This decouples the transfer process from the requirement for equipment-specific degradation data in existing few-shot RUL prediction methods, enabling the transfer of knowledge between domains from diverse and heterogeneous time series.

Nevertheless, time-series representation models for few-shot RUL prediction faces the following critical challenges:

- How to leverage widely used univariate time-series representation model to multivariate RUL prediction task? Currently, cross-domain time-series representation learning methods are often designed to capture temporal or spectral features of a single variable[18, 20, 21], where down-stream cross-variable dependencies are not and difficult to defined during pre-training. However, in practical applications, complex equipment status is typically characterized by multiple correlated sensor variables. This mismatch between pre-training and down-stream task requirements gives rise to the first challenge that must be addressed.
- How to design an effective fine-tuning strategy that guarantees stable convergence with extremely limited samples from target equipment for RUL prediction task? Current time-series representation models are parameter-intensive. In few-shot RUL prediction domain, natively fine-tuning all parameters not only leads to severe overfitting but may also substantially degrade the generalizable priors acquired during pre-training. The application of parameter-efficient finetuning approaches to multivariate RUL prediction has never been explored, which constitutes the second key challenge addressed.

Building on above discussion, this paper proposes PEFT-MuTS, a novel Parameter-Efficient Fine-Tuning framework for few-shot Multivariate Time-Series RUL prediction. PEFT-MuTS is built on a general time series representation model, which can be pre-trained on large-scale cross-domain time series data. Then, the pre-trained model is fine-tuned to adopt to the downstream RUL prediction task through an Independent Feature Tuning Network and Meta-Variable-based Low Rank Feature Fusion mechanism with minimal parameters. The main contributions of this paper are as follows:

- This paper demonstrates that cross-domain time-series representation models are highly effective for RUL prediction under extremely limited degradation data. By shifting the research focus from “identifying similar degradation patterns” to “leveraging generalizable temporal priors,” the proposed paradigm substantially broadens the scope of transferable source-domain data while simultaneously improving prediction accuracy, thereby offering a new perspective on the few-shot RUL prediction problem.
- A novel parameter-efficient fine-tuning framework, named PEFT-MuTS, is proposed for multivariate few-shot RUL prediction. PEFT-MuTS consists of an Independent Feature Tuning Network and a Meta-Variable-based

Low-Rank Feature Fusion mechanism. The former allows the univariate backbone to process each data variable independently, ensuring that representation capacity is not compromised by multivariate interactions. The latter introduces additional learnable meta-variable and employs a lightweight gated network with a small number of parameters to dynamically extract multivariate information, thereby achieving effective adaptation of univariate backbone networks to downstream multivariate RUL prediction tasks.

- The unstable phenomena of the fine-tuning process is analyzed in the case of extremely few samples, and a zero-initialized regressor is proposed as a simple yet effective solution to improve the fine-tuning stability, which provides a solid foundation for further researches based on pre-trained representation models for few-shot RUL prediction.

2. Related Works

2.1. Few-shot RUL Prediction Methods

In recent years, although data-driven RUL prediction methods have achieved high accuracy, their reliance on data quality and quantity remains a key challenge. With the rise of transfer learning, few-shot RUL prediction—particularly domain adaptation and meta-learning—has gained increasing attention.

Domain adaptation leverages labeled in-domain data to align source and target feature distributions through loss function constraints, enabling generalization to unlabeled target data[1]. Early approaches used adversarial training to address distribution shifts[9]. Wu et al.[11] further incorporated limited target labels to enhance adaptation. Ding et al.[7] adopted similar strategies for rotating machinery under condition-induced shifts. Cui et al.[6] employed digital twins to generate full-lifecycle synthetic source data, enabling adaptation to real-world few-shot targets. Li et al.[8] advanced this by removing source labels entirely, proposing a self-supervised framework. To address misalignment, Shang et al.[10] introduced a source distillation weighting mechanism that prioritizes source samples closer to the target domain.

Meta-learning aims to train models that generalize across tasks using few-shot data from multiple domains. A widely used approach is Model-Agnostic Meta-Learning (MAML), which learns a global parameter initialization that enables fast adaptation via support sets. Schmitt et al.[12] and Ding et al.[16] applied MAML to battery and variable-condition RUL prediction. Chang et al.[14] incorporated Bayesian modeling into MAML for uncertainty estimation. Cao et al.[13] applied MAML to wind turbine bearings by building support sets under varying conditions, while Zhuang et al.[17] used semantic attention with diverse-condition samples for cross-condition prediction.

Domain adaptation generally assumes the source and target domains share broad distribution similarities—e.g., data from similar equipments—limiting its applicability when source data are scarce. Likewise, MAML-based methods require meta-training tasks constructed from samples that cover sufficiently diverse degradation scenarios, and therefore still rely on a relatively amount of data from similar equipment. As a result, as discussed in the Section 1, existing methods primarily focus on identifying transferable degradation patterns of similar equipment under different operating conditions. When the available data from similar equipment are insufficient, the transfer process of such methods becomes inherently constrained. Recent advances in time series representation learning offer a promising way to address this limitation.

2.2. Time Series Representation Learning

Representation learning is a cornerstone of deep learning, enabling models to acquire task-agnostic high-level semantic features through self-supervised pre-training on large datasets, which are then transferred to downstream tasks to reduce data demand and improve convergence[20][19]. Due to the high variability of time series data, it is challenging to construct time series representation models with strong generalizability, and related research started relatively late. Notable approaches such as TF-C[19] aim to extract consistent and discriminative features from both the time and frequency domains, leveraging diverse augmentation strategies to enhance transferability across domains. TS2Vec[21] employs contrastive learning to generate positive and negative pairs from time series data, learning discriminative representations with strong transfer performance. SimMTM[18], grounded in manifold theory, uses masked modeling and learns consistent and diverse representations across two feature subspaces. Most recently, FEI[20] corrects inappropriate priors in contrastive-based time series representation models and builds a framework better suited for learning semantic continuity, thus improving generalization.

2.3. Parameter-efficient Fine-tuning

Although strong representation models enhance downstream transferability, preventing overfitting in low-data regimes becomes imperative, especially when adapting large pre-trained models. PEFT aims to improve fine-tuning performance with minimal additional parameters, and has become foundational in CV and NLP tasks[22]. Techniques like Side Tuning[23, 24, 25], Prompt(P)-Tuning[26, 27, 28] and LoRA[29, 30] are representative. However, most existing PEFT methods are developed primarily for the CV and NLP domains and are tightly coupled with standard Transformer architectures. For example, the widely used LoRA[29][30] fine-tuning strategy is almost exclusively tied to the MLP layers of Transformer architectures, while P-Tuning[26][27] and Prompt Tuning[28] are bound to the self-attention mechanism. In contrast, models for time-series representation learning and RUL prediction are not restricted to the standard Transformer paradigm and face a fundamental challenge arising from discrepancies in data variables between pre-training and downstream tasks[20]. Consequently, PEFT architectures tailored for multivariate RUL prediction based on time-series representation models remain underexplored and warrant further investigation.

3. Proposed Method

3.1. Formulation of the problem

Given a set of multivariate operational monitoring data $X \in \mathbb{R}^{B \times N \times T}$, where B is the number of available data samples, N is the number of monitored variables per device, and T is the time length of each sample, the corresponding device lifespans are denoted by $Y \in \mathbb{R}^B$. Here, the RUL label y_i is defined at the final timestamp T_i of each sample x_i .

Assuming the ideal full life-cycle length of a device is L , this study focuses on the scenario where $B \ll L$, indicating that the available monitoring data cannot fully cover the complete degradation process of the device.

In the standard data-driven RUL prediction framework, the training objective is typically defined as[31][32]:

$$\mathcal{L}(\theta, \phi) = \frac{1}{2B} \|Y - f_{\theta, \phi}(X)\|_2^2 \quad (1)$$

where:

$$f_{\theta, \phi}(X) = h_{\phi}(g_{\theta}(X)) \quad (2)$$

Here, g_{θ} denotes a randomly initialized feature extractor, and h_{ϕ} is a randomly initialized RUL regression head. Based on this setup, the proposed PEFT-MuTS architecture introduces a pre-trained backbone, a fine-tuning scheme, and a zero-initialized regression head for enhanced performance under limited degradation data.

3.2. PEFT-MuTS Framework

The overall architecture of PEFT-MuTS is illustrated in Fig. 1. PEFT-MuTS operates in two stages:

- Stage 1 conducts self-supervised pre-training of the backbone network g_{θ} using abundant and readily available cross-domain univariate time series data, leveraging existing methods such as FEI and SimMTM.
- Stage 2 performs fine-tuning, where the backbone network is adapted to the downstream RUL prediction task.

During the fine-tuning stage (Stage 2), the parameters of the pre-trained backbone network are frozen, and the PEFT-MuTS network is introduced as the tunable component for the backbone. Only the parameters of PEFT-MuTS are updated through gradient descent.

Specifically, a PEFT-MuTS network layer consists of an Independent Feature Tuning Network and a Meta-Variable-based Low-Rank Feature Fusion module, as illustrated in Fig. 2. In the figure, the green “Variable Path” denotes the processing path of the Independent Feature Tuning Network, which handles each data variable independently. The red “Meta-Variable Path” corresponds to the Low-Rank Feature Fusion, where information from different variables is aggregated.

The PEFT-MuTS layer performs feature extraction in parallel with the pre-trained backbone network, taking the same input as the backbone and feeding its activate output back into the backbone. The final output representation relies solely on the meta-variable features, which progressively fuse information from other data variables across layers. In addition, a “zero-initialized” regressor is introduced to stabilize fine-tuning under few-shot settings.

The computational details of each component are presented next. Section 3.2.1 introduces the Independent Feature Tuning Network, Section 3.2.2 describes the Meta-Variable-based Low-Rank Feature Fusion, and Section 3.3 analyzes the fine-tuning stability issue and addresses it through the proposed simple yet effective zero-initialized regressor.

Phase1: Cross-domain Self-supervised Pre-training

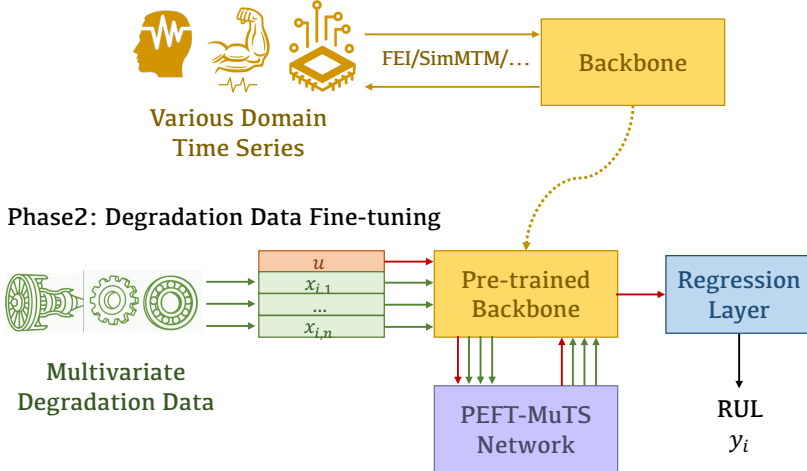


Figure 1: The Overall framework of the proposed PEFT-MuTS.

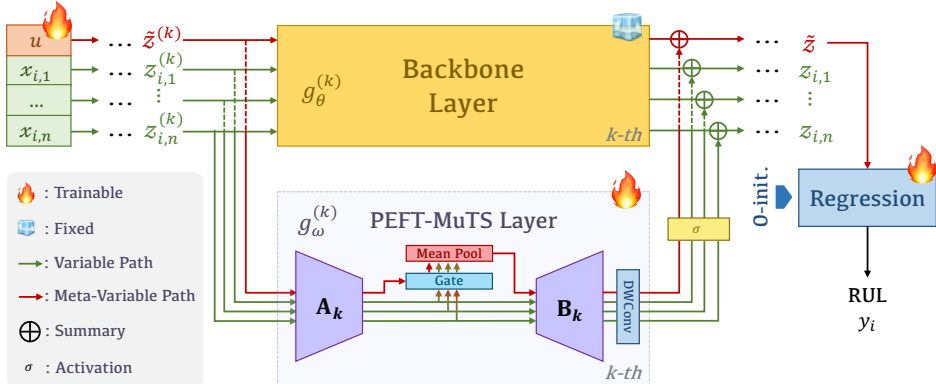


Figure 2: The details of PEFT-MuTS framework.

3.2.1. Independent Feature Tuning Network

The design of the Independent Feature Tuning Network is motivated by the need to preserve the univariate nature of the pre-trained time-series backbone. Since the backbone is pre-trained on univariate data, its prior structure is inherently tailored to feature extraction from a single time series. Naively introducing multivariate information would disrupt this pre-trained prior, potentially rendering the extracted features unreliable. Therefore, to preserve the backbone's prior structure while keeping the number of trainable parameters minimal during fine-tuning, an Independent Feature Tuning Network is introduced. This module enforces variable-wise feature extraction and employs low-rank mappings inspired by LoRA[29]. This module serves as the fundamental component for addressing challenge 1 discussed in the Section 1.

As illustrated in Fig. 2, given a multivariate degradation sample $x_i \in \mathbb{R}^{N \times T}$ with N variables, the computation at the k -th layer with the tuning module is as follows:

$$z_i^{(k+1)} = g_\theta^{(k)}(z_i^{(k)}) + \text{SiLU}(g_\omega^{(k)}(z_i^{(k)})) \quad (3)$$

where $z_i^{(k)} \in \mathbb{R}^{N \times d_k}$ is the intermediate feature at the k -th layer with dimension d_k , and $z_i^{(1)} = x_i$. SiLU represents the Sigmoid Linear Unit activation function[33], is used to regulate the overall information flow to the backbone layer and

is defined as:

$$\text{SiLU}(x) = x * \text{Sigmoid}(x) = x * \frac{1}{1 + e^{-x}} \quad (4)$$

$g_\theta^{(k)}$ denotes the k -th layer of the backbone, and $g_\omega^{(k)}$ is the corresponding tuning layer, defined as:

$$g_\omega^{(k)}(z_i^{(k)}) = \text{Conv} \left(z_i^{(k)} \mathbf{A}_k \mathbf{B}_k \right) \quad (5)$$

Here, $\mathbf{A}_k \in \mathbb{R}^{d_k \times r_k}$ and $\mathbf{B}_k \in \mathbb{R}^{r_k \times d_k}$ are the core parameters of the tuning module, where r_k denotes the projected dimension and is always much smaller than d_k , i.e., $r_k \ll d_k$. This low-rank mapping design ensures a minimal parameter overhead even under high-dimensional feature tuning. \mathbf{A}_k is randomly initialized, while \mathbf{B}_k is zero-initialized, encouraging the tuning output to start at zero and enabling residual learning that preserves pre-trained features and reduces overfitting.

3.2.2. Meta-Variable-based Low Rank Feature Fusion

As mentioned in the previous subsection, the Independent Feature Tuning Network ensures that the feature information of each variable is preserved during inter-layer propagation. However, how to achieve multivariate fusion on this basis is the focus of this subsection. To this end, we propose a Meta-Variable-based Low-Rank Feature Fusion mechanism to address Challenge 1 discussed in the Section 1, building upon the Independent Feature Tuning Network.

In this mechanism, we introduce an independently learned variable, referred to as a meta-variable, denoted by $u \in \mathbb{R}^{1 \times T}$. The meta-variable is specifically designed as a dedicated variable solely for information fusion. As part of the tunable parameters, it can be updated according to the requirements of the task and the backbone network. Within the low-rank space of PEFT-MuTS, this variable dynamically receives feature information from the data variables. This design preserves the independence of the data variables during their processing while ensuring that the features of u remain controllable during inter-layer propagation through its adjustable characteristics. Moreover, performing the fusion within a low-rank space keeps the number of fusion-related parameters manageable and promotes a more purposeful low-rank mapping \mathbf{A}_k , thereby constructing a subspace during optimization that is better suited for downstream tasks.

Denote the meta-variable as $u \in \mathbb{R}^{1 \times T}$, as illustrated by the red line in Figure 2. It is initialized as a zero vector with the same sequence length as the input x_i , enabling parallel processing with the input sequence: $\{u, x_i\} \in \mathbb{R}^{(N+1) \times T}$. Let the **low-rank representation** of the intermediate features of the data variables and the meta-variable be denoted as

$$v_i^{(k)} = \{\tilde{z}^{(k)}, z_i^{(k)}\} \mathbf{A}_k \in \mathbb{R}^{(N+1) \times r_k} \quad (6)$$

where $\tilde{z}^{(k)}$ represents the intermediate representation of the meta-variable u , with $\tilde{z}^{(1)} = u$. The processing of the meta-variable is then formulated as

$$\tilde{z}^{(k+1)} = g_\theta(\tilde{z}^{(k)}) + \text{SiLU}(f^{(k)}(v_i^{(k)}) \mathbf{B}_k) \quad (7)$$

where $f^{(k)}$ denotes the fusion function, defined by

$$f^{(k)}(v_i^{(k)}) = \text{MeanPool}(\text{Gate}(v_i^{(k)})) \quad (8)$$

Here, MeanPool represents an average pooling operation along the variable dimension with a window size of $N+1$, aggregating the filtered features of all data variables and the meta-variable. Gate is a self-gating mechanism that filters the intermediate features of all data variables and the meta-variable, selecting the parts used for multivariate fusion:

$$\text{Gate}(v_i^{(k)}) = \text{Sigmoid}(v_i^{(k)} \mathbf{W}_k) * v_i^{(k)} \quad (9)$$

where $\mathbf{W}_k \in \mathbb{R}^{r_k \times r_k}$ is a learnable parameter updated along with the model.

It should be noted that the above operations are applied exclusively to the intermediate variables of the meta-variable u . The resulting $\tilde{z}^{(k+1)}$ still only represents the updated meta-variable, while the data variables continue to follow the processing pipeline defined in Equation 5.

In this way, feature fusion of the data variables is achieved through the meta-variable u while maintaining the independent processing of each data variable. The gating mechanism constructs a flexible fusion path. The next subsection will analyze issues related to fine-tuning stability.

3.3. Zero-initialized RUL Regressor

In practice, we observe that fine-tuning pre-trained time series models on extremely small samples often results in highly unstable outcomes. Repeated training runs may yield significantly different results, and in some cases, the model may become trapped in poor local minima where the loss hardly decreases. To better understand this phenomenon, we conduct a variance-based analysis.

Consider the RUL prediction model trained with batch gradient descent as in (2). Given a linear regressor h_ϕ , where $\phi \sim \mathcal{N}(0, \sigma_\phi^2)$, and extracted degradation features $z \in \mathbb{R}^{B \times d}$ with $z \sim \mathcal{N}(0, \sigma_z^2)$, the prediction is $\hat{Y} = z\phi$, while the ground truth $Y \in \mathbb{R}^B$ is assumed to follow $Y \sim \mathcal{N}(0, \sigma_Y^2)$. Using the L_2 loss, the gradient update of the j -th parameter ϕ_j is:

$$\Delta\phi_j = -\eta \frac{\partial \mathcal{L}}{\partial \phi_j} = -\frac{\eta}{B} \sum_{i=1}^B z_{ij}(Y_i - z_i\phi) \quad (10)$$

Let $E_i = Y_i - z_i\phi$ be the prediction error. Since ϕ is randomly initialized, E_i is also a random variable. Its variance can be derived as:

$$\text{Var}(E_i) = \text{Var}(Y_i - z_i\phi) = \sigma_Y^2 + d \cdot \sigma_z^2 \cdot \sigma_\phi^2 \quad (11)$$

Then, the variance of the parameter update $\Delta\phi_j$ becomes:

$$\text{Var}(\Delta\phi_j) = \text{Var}\left(-\frac{\eta}{B} \sum_{i=1}^B z_{ij} E_i\right) = \frac{\eta^2}{B^2} \sum_{i=1}^B \text{Var}(z_{ij} E_i) \quad (12)$$

For simplicity, assuming independence between z_{ij} and E_i , we have:

$$\text{Var}(z_{ij} E_i) = \text{Var}(z_{ij}) \cdot \text{Var}(E_i) = \sigma_z^2 \cdot (\sigma_Y^2 + d \cdot \sigma_z^2 \cdot \sigma_\phi^2) \quad (13)$$

Thus:

$$\text{Var}(\Delta\phi_j) = \frac{\eta^2}{B} \cdot \sigma_z^2 \cdot (\sigma_Y^2 + d \cdot \sigma_z^2 \cdot \sigma_\phi^2) \quad (14)$$

This analysis shows that the gradient variance is positively correlated with the variance of the input features σ_z^2 , the label variance σ_Y^2 , and the initialization variance of the regressor σ_ϕ^2 . A large update variance leads to strong randomness in the early training stage, manifesting as instability across different training runs.

Notably, since pre-trained representation models produce more discriminative features in the early stage of fine-tuning, the initial feature variance σ_z^2 is usually high. This leads to larger $\text{Var}(\Delta\phi)$ and hence greater instability compared to training from scratch.

To suppress this effect, we adopt zero-initialized regressor in PEFT-MuTS, i.e., $\phi = \mathbf{0}$, which yields the minimal initial gradient variance:

$$\text{Var}(\Delta\phi_j) = \frac{\eta^2}{B^2} \cdot \sigma_z^2 \cdot \sigma_Y^2 \quad (15)$$

This eliminates the contribution of σ_ϕ^2 , thereby avoiding additional instability caused by common initializers such as Xavier[34] or Kaiming[35], and significantly reduces the impact of σ_z^2 .

Based on this analysis, a zero-initialized regressor is introduced to address this issue, thereby resolving Challenge 2 discussed in Section 1. In subsequent experiments, we empirically validate the effectiveness of zero-initialized regressor in improving fine-tuning stability.

4. Experiments

4.1. Preparing Datasets

4.1.1. Basic informations

This study employs two widely-used prognostic datasets: the C-MAPSS dataset[36] for aircraft engine degradation and the XJTU-SY Bearing dataset[37] for bearing degradation. For the C-MAPSS dataset, we adopt the FD002 and FD004 subsets, which contain six operating conditions and reflect more realistic and complex scenarios. We select 14 commonly used variables that exhibit degradation trends[31]. More details about the C-MAPSS dataset can be found in reference [36]. For the Bearing dataset, we use all three operating condition subsets, denoted as OP-A, OP-B, and OP-C, which correspond to different speeds and loads. Each instance includes vibration signals in both horizontal and vertical directions. More details are available in [37][38].

4.1.2. RUL Labels

For the C-MAPSS dataset, we adopt the commonly used piecewise linear labeling method[31]. The degradation start point is defined as 120 cycles before failure. Prior to this point, the unit is considered healthy, and RUL degrades linearly afterward. For the Bearing dataset, we follow Su et al. [39][14] and use the root mean square (RMS) method combined with the 3-sigma rule to determine the degradation onset. Similarly, a linear degradation is assumed after the degradation point. All RUL labels are normalized to the range [0, 1], where 1 denotes the healthy state and 0 denotes failure[14][31].

4.1.3. Construction of Small Degradation Sample Datasets

Based on the above datasets, we construct small-sample degradation datasets of varying scales using the following three-step procedure:

First, a sliding window of fixed length is applied to generate time series segments, with the RUL assigned as the value at the last time step. This creates sample-label pairs across the full degradation cycle. For C-MAPSS, the window size is 30 with a step of 15; for the Bearing dataset, the window size is 1024 with a step of 32768.

We then perform three levels of sampling:

1. **Device Retention Percentage p_1** : For datasets with multiple device units (e.g., C-MAPSS), we retain entire device units with probability p_1 , discarding samples from unselected devices. This step is applied only to C-MAPSS. For the Bearing dataset, which contains only 5 units per condition (OP-A/B/C), we directly use the first unit from each condition.
2. **RUL Coverage Percentage p_2** : A subset of RUL labels is randomly selected with probability p_2 (without replacement). All samples corresponding to the selected RULs are retained. Healthy samples (RUL = 1) are always preserved, given their abundance and accessibility in real scenarios.
3. **Global Data Retention Percentage p_3** : To introduce additional randomness and better simulate real-world conditions, we further sample from the filtered data with probability p_3 . A smaller p_3 yields fewer total samples.

Table 1 summarizes the resulting small-sample training sets. Since the OP-A operating condition in the Bearing dataset contains relatively few samples, we divide this condition into only two few-shot scenarios. In the Data Proportion columns, the Device, RUL, and Global Retention values indicate the respective percentages, while the Total column shows the overall percentage of each subset relative to the original dataset. In the Number of Samples columns, Early Stage, Middle Stage, and Late Stage report the number of samples with RUL < 1, divided into RUL $\in [0.7, 1.0]$, RUL $\in [0.3, 0.7]$, and RUL $\in [0.0, 0.3]$ respectively. The Health Stage column indicates the number of samples with RUL = 1.

4.1.4. Test Sets

The datasets in Table 1 are used for training. For testing, we use the original test sets. FD002 contains 259 test engine instances, and FD004 has 248 test engines, all with incomplete degradation. For the Bearing dataset, we use all remaining bearings (units 2-5) from OP-A, OP-B, and OP-C as the test set. No additional processing is performed on test sets, and window sizes and step lengths are consistent with the training set.

Table 1

Dataset statistics with varying proportions.

Dataset	Data Percentage				Number of Training Samples at Each Stage			
	Device p_1	RUL p_2	Global p_3	Total	Early	Middle	Late	Health
FD002-1	30%	3%	80%	0.72%	0	8	5	270
FD002-2	30%	8%	80%	1.92%	0	11	28	220
FD002-3	30%	30%	80%	7.20%	37	54	44	243
FD002-4	30%	60%	80%	14.40%	100	114	76	248
FD004-1	30%	3%	80%	0.72%	0	2	8	371
FD004-2	30%	8%	80%	1.92%	6	12	25	337
FD004-3	30%	30%	80%	7.20%	54	40	34	335
FD004-4	30%	60%	80%	14.40%	67	129	95	327
OP-A-1	/	5%	100%	5%	0	0	1	77
OP-A-2	/	10%	100%	10%	0	1	2	77
OP-B-1	/	10%	10%	1%	0	0	1	44
OP-B-2	/	10%	50%	5%	1	0	1	226
OP-B-3	/	10%	100%	10%	0	1	1	454
OP-C-1	/	10%	10%	1%	0	0	1	33
OP-C-2	/	10%	50%	5%	0	1	1	169
OP-C-3	/	10%	100%	10%	0	1	1	340

Table 2

PEFT-MuTS structure details with ResNet-18 Backbone.

Layers	d_k	r_k	DWConv
Input Embedding	N	/	/
Block1	64	128	128
Block2	128	32	/
Block3	128	32	256
Block4	256	4	/
Block5	256	4	512
Block6	512	2	/
Block7	512	2	1024
Block8	1024	1	/
Total Params	15M	74.9K(0.50%)	

4.1.5. Normalization

Following standard practice, we apply min-max normalization to all datasets. Each independently constructed small-sample training set is normalized separately, using its own min and max values. These values are then applied to normalize the corresponding test set to prevent information leakage during training.

4.2. Implementation Details

PEFT-MuTS employs a 1-D ResNet-18 backbone that has been pre-trained using the FEI method [20]. The pre-training configuration strictly follows the original paper’s settings, and the process is conducted on the SleepEEG dataset[40]. The training set of this dataset contains 371,055 EEG signal samples, each with a length of 178, covering a total of 66,047,790 time points, sampled at 100 Hz. This dataset exhibits rich temporal variation semantics and abundant spectral information, and has been widely adopted as a benchmark dataset for time-series pretraining[18][19][20]. Therefore, it is also used as the pretraining dataset in this work, in alignment with the experimental setting of FEI[20].

Each residual block of ResNet-18 (excluding the input embedding layer) is followed by a PEFT-MuTS layer. As each block has 2 convolutional layers (excluding shortcuts), 8 PEFT-MuTS layers are attached in total. Table2 details each module: **Layers** denotes the corresponding backbone block, d_k is the input feature dimension of the block, which is also the input dimension to the PEFT-MuTS layer, r_k is its inner projection dimension, and **DWConv** specifies the number of depthwise separable kernels (kernel size 3) for dimensional alignment when needed. This setup adds only 74.9K parameters—just 0.50% of the backbone.

Table 3

Comparison of RUL prediction performance on small-sample C-MAPSS datasets across different methods.

Methods	Metrics	FD002-1	FD002-2	FD002-3	FD002-4	FD004-1	FD004-2	FD004-3	FD004-4
PEFT-MuTS	MAE	0.1529 \pm 0.01	0.1391 \pm 0.00	0.1467 \pm 0.01	0.1573 \pm 0.00	0.1072 \pm 0.00	0.1225 \pm 0.01	0.1222 \pm 0.00	0.1469 \pm 0.01
	MAPE(%)	38.382 \pm 2.28	28.280 \pm 0.73	27.050 \pm 0.80	26.410 \pm 0.45	26.582 \pm 0.75	26.828 \pm 0.81	23.302 \pm 0.88	22.976 \pm 0.29
	RMSE	0.2415 \pm 0.01	0.2042 \pm 0.00	0.2084 \pm 0.01	0.1922 \pm 0.01	0.2082 \pm 0.00	0.2078 \pm 0.00	0.1907 \pm 0.00	0.2047 \pm 0.00
Full	MAE	0.1831 \pm 0.01	0.1821 \pm 0.02	0.1861 \pm 0.01	0.1792 \pm 0.01	0.1228 \pm 0.00	0.1434 \pm 0.01	0.1417 \pm 0.00	0.1748 \pm 0.00
	MAPE(%)	47.466 \pm 1.01	35.688 \pm 3.90	32.160 \pm 0.77	28.476 \pm 0.53	30.870 \pm 0.65	29.418 \pm 1.56	24.726 \pm 0.74	26.192 \pm 0.33
	RMSE	0.2756 \pm 0.01	0.2395 \pm 0.02	0.2344 \pm 0.01	0.2259 \pm 0.01	0.2242 \pm 0.00	0.2123 \pm 0.01	0.1942 \pm 0.00	0.2247 \pm 0.01
Transfer Learning	MAE	0.1872 \pm 0.00	0.1952 \pm 0.01	0.2141 \pm 0.00	0.2304 \pm 0.01	0.1388 \pm 0.01	0.1497 \pm 0.00	0.1884 \pm 0.01	0.2233 \pm 0.04
	MAPE(%)	50.544 \pm 0.85	49.638 \pm 1.98	42.502 \pm 0.57	41.292 \pm 0.74	34.678 \pm 0.91	34.388 \pm 0.43	33.828 \pm 0.42	34.828 \pm 2.22
	RMSE	0.2888 \pm 0.01	0.2823 \pm 0.01	0.2644 \pm 0.00	0.2710 \pm 0.01	0.2430 \pm 0.01	0.2342 \pm 0.00	0.2351 \pm 0.01	0.2707 \pm 0.04
DTL[25]	MAE	0.2078 \pm 0.00	0.2015 \pm 0.01	0.1972 \pm 0.00	0.2005 \pm 0.00	0.1593 \pm 0.01	0.1900 \pm 0.01	0.1685 \pm 0.01	0.2014 \pm 0.01
	MAPE(%)	50.202 \pm 1.05	35.672 \pm 1.36	33.040 \pm 0.90	31.4900 \pm 0.36	34.1940 \pm 1.04	33.9540 \pm 1.26	27.6220 \pm 1.41	29.534 \pm 0.89
	RMSE	0.2914 \pm 0.01	0.2560 \pm 0.01	0.2480 \pm 0.00	0.2511 \pm 0.00	0.2376 \pm 0.01	0.2498 \pm 0.01	0.2202 \pm 0.01	0.2551 \pm 0.01
MKDPINN[41]	MAE	0.1581 \pm 0.03	0.1427 \pm 0.01	0.1629 \pm 0.01	0.1641 \pm 0.01	0.1241 \pm 0.03	0.1382 \pm 0.00	0.1383 \pm 0.01	0.1557 \pm 0.00
	MAPE(%)	45.070 \pm 0.80	36.950 \pm 0.41	29.070 \pm 1.66	27.320 \pm 1.32	30.930 \pm 0.45	29.760 \pm 0.60	24.130 \pm 0.72	21.580 \pm 0.41
	RMSE	0.2626 \pm 0.05	0.2267 \pm 0.02	0.2076 \pm 0.01	0.1981 \pm 0.01	0.2298 \pm 0.01	0.2161 \pm 0.00	0.1997 \pm 0.02	0.1915 \pm 0.01
TACDA[42]	MAE	0.3653 \pm 0.05	0.5506 \pm 0.03	0.4029 \pm 0.07	0.3615 \pm 0.03	0.2876 \pm 0.02	0.5355 \pm 0.07	0.4369 \pm 0.01	0.3213 \pm 0.03
	MAPE(%)	48.950 \pm 0.77	64.060 \pm 2.52	51.380 \pm 1.05	48.700 \pm 0.72	40.000 \pm 0.80	59.490 \pm 1.30	50.800 \pm 0.33	42.140 \pm 1.71
	RMSE	0.3979 \pm 0.03	0.5943 \pm 0.05	0.4390 \pm 0.05	0.3932 \pm 0.02	0.3038 \pm 0.04	0.5667 \pm 0.02	0.4633 \pm 0.07	0.3392 \pm 0.04
ResNet-18[43]	MAE	0.2093 \pm 0.00	0.2190 \pm 0.03	0.2067 \pm 0.01	0.1916 \pm 0.00	0.1526 \pm 0.00	0.1792 \pm 0.00	0.1572 \pm 0.00	0.1928 \pm 0.01
	MAPE(%)	51.466 \pm 0.72	43.014 \pm 7.01	37.330 \pm 1.59	31.370 \pm 0.27	34.850 \pm 0.44	34.838 \pm 0.87	27.406 \pm 0.62	28.376 \pm 0.54
	RMSE	0.2963 \pm 0.00	0.2825 \pm 0.04	0.2588 \pm 0.01	0.2391 \pm 0.00	0.2403 \pm 0.00	0.2460 \pm 0.01	0.2088 \pm 0.00	0.2434 \pm 0.01
DAMCNN[38]	MAE	0.1802 \pm 0.00	0.2192 \pm 0.01	0.2195 \pm 0.00	0.2317 \pm 0.01	0.1254 \pm 0.00	0.1410 \pm 0.00	0.1709 \pm 0.00	0.1995 \pm 0.01
	MAPE(%)	50.080 \pm 0.34	49.092 \pm 1.35	46.480 \pm 0.37	43.034 \pm 1.41	33.476 \pm 0.10	33.916 \pm 0.20	34.720 \pm 0.38	32.132 \pm 0.81
	RMSE	0.2909 \pm 0.00	0.3132 \pm 0.01	0.2957 \pm 0.00	0.3005 \pm 0.01	0.2443 \pm 0.00	0.2430 \pm 0.00	0.2549 \pm 0.01	0.2751 \pm 0.01
Dual-Mixer[31]	MAE	0.2353 \pm 0.00	0.2831 \pm 0.01	0.2548 \pm 0.01	0.2407 \pm 0.02	0.1828 \pm 0.01	0.2138 \pm 0.01	0.2274 \pm 0.01	0.2350 \pm 0.01
	MAPE(%)	55.010 \pm 0.77	54.500 \pm 2.11	45.872 \pm 2.53	40.376 \pm 3.41	39.130 \pm 0.81	40.040 \pm 1.32	38.172 \pm 1.15	33.874 \pm 1.08
	RMSE	0.3209 \pm 0.01	0.3590 \pm 0.02	0.3192 \pm 0.01	0.2986 \pm 0.02	0.2684 \pm 0.01	0.2846 \pm 0.01	0.2901 \pm 0.01	0.2922 \pm 0.01
IMDSSN[32]	MAE	0.1934 \pm 0.01	0.2232 \pm 0.01	0.2219 \pm 0.01	0.2269 \pm 0.05	0.1494 \pm 0.01	0.1629 \pm 0.01	0.1830 \pm 0.02	0.1844 \pm 0.01
	MAPE(%)	51.398 \pm 1.35	52.036 \pm 2.39	43.828 \pm 2.82	40.680 \pm 6.11	36.300 \pm 1.33	35.854 \pm 0.58	33.894 \pm 1.43	28.278 \pm 0.25
	RMSE	0.2936 \pm 0.01	0.3034 \pm 0.01	0.2733 \pm 0.00	0.2697 \pm 0.04	0.2525 \pm 0.01	0.2452 \pm 0.00	0.2354 \pm 0.01	0.2329 \pm 0.00

Fine-tuning is conducted for 300 epochs. Due to the extremely small sample size, a validation set is not partitioned, and thus early stopping based on validation loss is not employed. The optimizer used is AdamW with $\beta = (0.9, 0.999)$, an initial learning rate of 0.001, an exponential decay rate of 0.99, and a maximum batch size of 8.

4.3. Experimental Results

4.3.1. Baselines

We select several supervised learning methods for RUL prediction as baselines, including Dual-Mixer[31], DAMCNN[38], IMDSSN[32] and ResNet[43], to compare the proposed method with conventional supervised approaches in terms of predictive performance. In addition, we introduce state-of-art domain adaptation method designed for few-shot scenarios TACDA[42] and a meta-learning-based few-shot RUL prediction method MKDPINN[41] to evaluate the performance of traditional few-shot learning paradigms under extremely limited data conditions. Furthermore, an Side-Tuning-based fine-tuning framework DTL[25] is incorporated to compare the proposed fine-tuning strategy with existing Side Tuning-based approaches in multivariate RUL prediction scenarios. On this basis, standard fine-tuning strategies are further included as fundamental baselines, namely full fine-tuning (Full) and linear fine-tuning (Linear), to verify the performance gains obtained from the pre-training stage.

4.3.2. Evaluation Metrics

We employ MAE, RMSE, and MAPE as performance evaluation metrics. For the Bearing dataset, due to the presence of numerous samples with zero RUL in the test set, we replace MAPE with SMAPE to avoid numerical explosion caused by division by zero. The formulation these matrices are as follow:

$$\text{MAE} = \frac{1}{n} \sum_{i=1}^n |y_i - \hat{y}_i| \quad (16)$$

Table 4

Comparison of RUL prediction performance on small-sample XJTU-SY Bearing datasets across different methods.

Methods	Metrics	OP-A-1	OP-A-2	OP-B-1	OP-B-2	OP-B-3	OP-C-1	OP-C-2	OP-C-3
PEFT-MuTS	MAE	0.1541 ± 0.01	0.1536 ± 0.01	0.1270 ± 0.01	0.1161 ± 0.03	0.1962 ± 0.04	0.0987 ± 0.00	0.0990 ± 0.01	0.0985 ± 0.00
	SMAPE(%)	19.672 ± 3.88	18.215 ± 2.64	18.858 ± 1.49	12.953 ± 1.52	17.392 ± 1.88	8.827 ± 0.29	8.637 ± 0.24	8.551 ± 0.17
	RMSE	0.2372 ± 0.01	0.2379 ± 0.01	0.1738 ± 0.02	0.2038 ± 0.06	0.3296 ± 0.07	0.1616 ± 0.01	0.1898 ± 0.02	0.1986 ± 0.01
Full	MAE	0.1661 ± 0.02	0.1728 ± 0.02	0.2021 ± 0.08	0.2180 ± 0.30	0.1121 ± 0.02	0.1088 ± 0.01	0.1194 ± 0.01	0.1067 ± 0.05
	SMAPE(%)	18.410 ± 1.55	20.539 ± 5.32	24.982 ± 8.79	15.231 ± 6.47	16.346 ± 4.92	9.712 ± 0.62	9.964 ± 1.04	8.612 ± 1.32
	RMSE	0.2564 ± 0.02	0.2705 ± 0.03	0.3069 ± 0.11	0.3849 ± 0.58	0.1607 ± 0.03	0.1989 ± 0.03	0.2392 ± 0.02	0.2828 ± 0.22
Transfer Learning	MAE	0.2288 ± 0.06	0.1747 ± 0.03	0.1943 ± 0.05	0.1168 ± 0.02	0.2912 ± 0.12	0.1505 ± 0.03	0.1165 ± 0.01	0.1175 ± 0.02
	SMAPE(%)	26.249 ± 4.55	20.000 ± 4.77	23.008 ± 5.99	14.875 ± 1.78	22.734 ± 4.41	11.366 ± 1.69	9.882 ± 1.05	9.883 ± 1.31
	RMSE	0.3352 ± 0.13	0.2363 ± 0.03	0.2629 ± 0.06	0.1775 ± 0.03	0.4401 ± 0.19	0.2204 ± 0.04	0.1838 ± 0.02	0.1895 ± 0.06
DTL[25]	MAE	0.2331 ± 0.04	0.1797 ± 0.02	0.1910 ± 0.00	0.3097 ± 0.21	0.4033 ± 0.36	0.2634 ± 0.09	0.1075 ± 0.01	0.0918 ± 0.01
	SMAPE(%)	20.900 ± 0.81	18.390 ± 1.30	16.080 ± 2.95	19.498 ± 5.74	20.652 ± 7.44	15.796 ± 3.03	9.934 ± 0.50	8.498 ± 0.85
	RMSE	0.3482 ± 0.09	0.2520 ± 0.03	0.2484 ± 0.01	0.5242 ± 0.39	0.6854 ± 0.64	0.3211 ± 0.10	0.1963 ± 0.03	0.1629 ± 0.02
MKDPINN[41]	MAE	0.2143 ± 0.10	0.1670 ± 0.21	0.1968 ± 0.11	0.2593 ± 0.09	0.2257 ± 0.17	0.1161 ± 0.15	0.1269 ± 0.09	0.1182 ± 0.12
	SMAPE(%)	19.930 ± 1.07	12.810 ± 0.84	22.680 ± 2.01	20.370 ± 1.73	19.120 ± 2.15	9.160 ± 0.98	9.610 ± 0.64	9.130 ± 1.82
	RMSE	0.3194 ± 0.03	0.2063 ± 0.01	0.2568 ± 0.06	0.4070 ± 0.01	0.3583 ± 0.04	0.2591 ± 0.05	0.2737 ± 0.01	0.2803 ± 0.01
TACDA[42]	MAE	0.2848 ± 0.23	0.2806 ± 0.34	0.4418 ± 0.16	0.2732 ± 0.20	0.2424 ± 0.20	0.8250 ± 0.33	0.2204 ± 0.07	0.1957 ± 0.11
	SMAPE(%)	23.860 ± 1.11	23.580 ± 0.92	39.010 ± 2.65	22.210 ± 2.70	20.080 ± 0.86	84.800 ± 8.13	15.240 ± 0.55	13.670 ± 0.90
	RMSE	0.3384 ± 0.04	0.3372 ± 0.08	0.4944 ± 0.08	0.3322 ± 0.11	0.3388 ± 0.06	0.8625 ± 0.62	0.2616 ± 0.09	0.2551 ± 0.05
ResNet-18[43]	MAE	0.2061 ± 0.03	0.1821 ± 0.02	1.1122 ± 0.76	0.5743 ± 0.52	0.2489 ± 0.24	0.1877 ± 0.07	0.1468 ± 0.08	0.0937 ± 0.01
	SMAPE(%)	26.054 ± 4.72	22.812 ± 2.72	44.166 ± 18.41	25.765 ± 11.88	21.941 ± 4.08	13.450 ± 3.85	10.055 ± 2.40	8.597 ± 0.71
	RMSE	0.3251 ± 0.05	0.2900 ± 0.03	1.7024 ± 1.15	1.0705 ± 0.98	0.3925 ± 0.43	0.3585 ± 0.10	0.3663 ± 0.26	0.1801 ± 0.02
DAMCNN[38]	MAE	0.2669 ± 0.04	0.2672 ± 0.02	0.2224 ± 0.03	0.1991 ± 0.07	0.1869 ± 0.05	0.1777 ± 0.06	0.1204 ± 0.00	0.1203 ± 0.01
	SMAPE(%)	22.115 ± 1.79	22.096 ± 0.98	21.207 ± 3.30	17.555 ± 3.22	17.661 ± 1.76	13.202 ± 2.93	9.328 ± 0.14	9.294 ± 0.31
	RMSE	0.3811 ± 0.05	0.3855 ± 0.01	0.3222 ± 0.02	0.3082 ± 0.11	0.2934 ± 0.09	0.2554 ± 0.05	0.2682 ± 0.01	0.2706 ± 0.01
Dual-Mixer[31]	MAE	0.9226 ± 0.07	0.8635 ± 0.20	0.8010 ± 0.43	0.3484 ± 0.09	0.4084 ± 0.15	1.1707 ± 0.12	0.4324 ± 0.09	0.3342 ± 0.02
	SMAPE(%)	41.473 ± 1.09	39.988 ± 4.75	39.730 ± 7.10	25.347 ± 1.88	27.259 ± 3.46	39.799 ± 2.38	21.701 ± 2.72	18.700 ± 0.65
	RMSE	1.0493 ± 0.11	0.9841 ± 0.21	0.9421 ± 0.43	0.4406 ± 0.11	0.5202 ± 0.18	1.3044 ± 0.11	0.5308 ± 0.09	0.4340 ± 0.04
IMDSSN[32]	MAE	3.9874 ± 3.40	1.6401 ± 0.73	5.1916 ± 2.80	3.1417 ± 1.25	2.1069 ± 0.80	1.9114 ± 0.28	1.3881 ± 0.56	0.8120 ± 0.31
	SMAPE(%)	66.552 ± 12.2	58.360 ± 7.87	71.854 ± 12.5	64.163 ± 8.01	58.784 ± 5.50	55.090 ± 3.30	47.662 ± 5.83	38.066 ± 5.29
	RMSE	5.9707 ± 5.10	2.2283 ± 1.02	7.1127 ± 3.64	4.4466 ± 1.69	3.0528 ± 1.13	2.9479 ± 0.59	1.9058 ± 0.73	1.1510 ± 0.35

$$\text{RMSE} = \sqrt{\frac{1}{n} \sum_{i=1}^n (y_i - \hat{y}_i)^2} \quad (17)$$

$$\text{MAPE} = \frac{100\%}{n} \sum_{i=1}^n \left| \frac{y_i - \hat{y}_i}{y_i} \right| \quad (18)$$

$$\text{SMAPE} = \frac{100\%}{n} \sum_{i=1}^n \frac{|y_i - \hat{y}_i|}{(|y_i| + |\hat{y}_i|)/2} \quad (19)$$

4.3.3. Results and Analysis

The overall comparative results on all few-shot datasets are presented in Table 3 and Table 4. Each reported result includes the mean and standard deviation over 5 repeated experiments.

The results reported in the table suggest that the pre-trained PEFT-MuTS, Linear, Full, and DTL models tend to outperform conventional supervised learning methods across nearly all evaluation metrics. This observation indicates that, even when the pre-training dataset is not directly related to the RUL prediction task, self-supervised pre-training based on learning general temporal representations, rather than task-specific degradation knowledge, may still lead to performance improvements in few-shot RUL prediction.

From the results, the only difference between the Full and ResNet-18 models is that the former leverages FEI pre-training, while the latter uses standard random initialization. Therefore, comparing these two reveals that even without additional fine-tuning structures, full fine-tuning of a pre-trained representation model significantly benefits few-shot

RUL prediction, clearly outperforming the randomly initialized ResNet-18. This highlights the inherent value of cross-domain temporal knowledge for data-driven RUL prediction tasks. However, the large number of parameters involved in full fine-tuning (approximately 15M) results in excessive optimization freedom, which may lead to overfitting risks in few-shot scenarios, and thus its performance is not fully unleashed.

In contrast, the Linear approach only fine-tunes the output layer (a single linear regression layer), drastically reducing the number of trainable parameters to 1024. Even with such a limited capacity, it still outperforms several conventional supervised learning methods in most scenarios by leveraging the pre-trained representation model. When compared to the randomly initialized 15M-parameter ResNet-18, the Linear method achieves comparable or even superior performance in some cases, further emphasizing the effectiveness of the pre-trained backbone. However, its extremely low flexibility hinders its ability to adapt to specific tasks, making it noticeably inferior to the full fine-tuning method.

PEFT-MuTS and DTL achieve a more favorable balance between parameter efficiency and predictive performance, significantly improving fine-tuning efficiency. Compared with the Linear strategy, they introduce a modest increase in the number of trainable parameters while substantially enhancing the model's adaptability in few-shot scenarios. Moreover, PEFT-MuTS incorporates a dedicated multivariate fusion mechanism in its architecture, enabling more effective utilization of multivariate information during fine-tuning. As a result, PEFT-MuTS consistently outperforms DTL with a clear performance margin.

In addition, it can be observed that the meta-learning-based MKDPINN exhibits unstable performance under extreme few-shot conditions, particularly on the FD002-1, FD002-2, FD004-1, OP-B-1, and OP-B-2 datasets. Although its performance significantly surpasses that of conventional supervised learning methods, it still lags behind self-supervised pre-training-based approaches. Domain adaptation methods perform even worse in these settings. The underlying reason is that such methods heavily rely on the availability of data from known similar equipment or operating conditions. When the number of samples is extremely limited, the prior knowledge provided by these datasets becomes insufficient, severely constraining the transfer process. In contrast, self-supervised learning methods directly learn task-agnostic and transferable representations from large-scale datasets. The improved generalization capability of these representations effectively reduces the difficulty of adapting to downstream tasks, without relying exclusively on observable similar equipment or operating conditions. Nevertheless, pre-trained representations alone are not sufficient. The multivariate fusion mechanism specifically designed in PEFT-MuTS ensures more effective information utilization during adaptation, which is particularly beneficial for datasets with a large number of variables, such as CMAPSS.

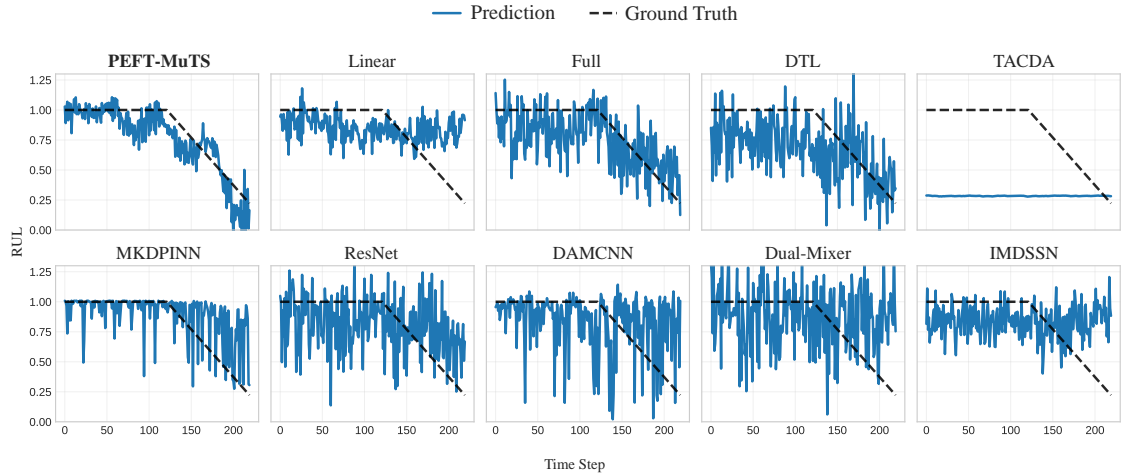
Figures 3a and 3b present representative prediction results of different models on the FD002-2 dataset and the OP-A-1 bearing dataset, respectively. On FD002-2, PEFT-MuTS is able to more accurately model degradation characteristics across the early, middle, and late stages. Due to the scarcity of degradation samples and the predominance of healthy samples, most models exhibit a strong bias toward predicting the healthy stage. Except for the pre-trained Full fine-tuning and DTL methods, which retain limited predictive capability, the remaining models fail to effectively capture degradation trends. On the OP-A-1 dataset, benefiting from the strong generalization ability of the pre-trained model, PEFT-MuTS, Full fine-tuning, DTL, and even Linear fine-tuning achieve more accurate predictions for previously unseen mid-stage degradation samples. In contrast, the randomly initialized ResNet-18 tends to classify all mid- and late-stage degradation samples as late-stage degradation, while DAMCNN shows a strong bias toward early-stage degradation; neither is capable of accurately modeling the mid-stage degradation process. Dual-Mixer and IMDSSN are overly sensitive to noise in vibration signals, resulting in highly fluctuating outputs with little practical predictive value. The domain adaptation method TACDA completely fails under this setting, and the meta-learning-based MKDPINN also delivers unsatisfactory performance.

4.4. Model Analysis

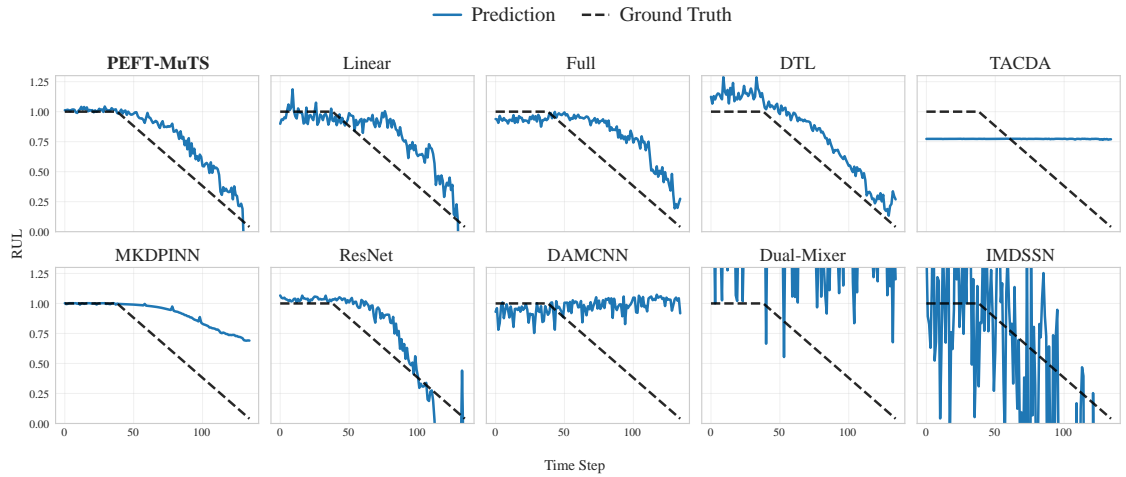
4.4.1. Ablation Study Design

To evaluate the effectiveness of PEFT-MuTS components, we conduct ablation studies focusing on: (1) cross-domain pre-training of the backbone (**pre-train**), (2) meta-variable low rank multivariate fusion (**meta-variable**), and (3) zero-initialized regression head (**zero-init.**). By selectively enabling or disabling these modules, we construct five variant models.

Specifically, the **pre-train** setting uses ResNet-18 pre-trained on SleepEEG via the FEI strategy; its removal means using a randomly initialized backbone. The **meta-variable** module introduces meta-variable u to integrate multivariate



(a) The prediction results of the comparision methods on the 1# test engine unit of FD002-2 dataset.



(b) The prediction results of the comparision methods on the 2# bearing of OP-A-1 dataset.

Figure 3: The visualization of prediction results on C-MAPSS and Bearing datasets.

features as in Eq. 7; without it, features are averaged before output. The **zero-init.** setting uses a zero-initialized linear regressor; otherwise, a bias-free Kaiming-initialized layer is applied.

4.4.2. Ablation Results and Analysis

The ablation results are shown in Table 5. Several key findings emerge:

1. **Cross-domain pre-training:** The cross-domain pre-training of the backbone significantly improves performance on the few-shot RUL prediction task. Removing this component leads to notable degradation across all datasets. However, its effectiveness depends on complementary designs that account for multivariate fusion and training stability (i.e., zero-initialized regression). The meta-variable low rank fusion and zero-initialized regressor proposed in this work synergize with pre-training and together yield substantial improvements under extreme few-shot conditions.
2. **Multivariate fusion:** The meta-variable-based low rank fusion method proposed in PEFT-MuTS consistently improves prediction performance across almost all datasets. On the Bearing dataset, the improvement is relatively limited, which is attributed to the small number of variables and the modest inter-variable correlations—where single-variable features already provide sufficient information for modeling degradation. This suggests that RUL

Table 5

The ablation study results.

Components	Metrics	FD002-1	FD004-1	OP-A-1	OP-B-1	OP-C-1
pre-train ✓ meta-variable ✓ zero-init. ✓	MAE (S)MAPE(%) RMSE	0.1529 \pm 0.01 38.382 \pm 2.28 0.2415 \pm 0.01	0.1072 \pm 0.00 26.582 \pm 0.75 0.2082 \pm 0.00	0.1541 \pm 0.01 19.672 \pm 3.88 0.2372 \pm 0.02	0.1270 \pm 0.01 18.858 \pm 1.49 0.1738 \pm 0.02	0.0987 \pm 0.00 8.827 \pm 0.29 0.1616 \pm 0.01
✓ ✓ ✗	MAE (S)MAPE(%) RMSE	0.1697 \pm 0.01 42.806 \pm 1.52 0.2531 \pm 0.01	0.1243 \pm 0.01 29.646 \pm 1.75 0.2156 \pm 0.01	0.2041 \pm 0.04 24.538 \pm 5.50 0.3030 \pm 0.06	0.1791 \pm 0.06 23.894 \pm 8.20 0.2433 \pm 0.08	0.1396 \pm 0.01 10.738 \pm 0.49 0.2163 \pm 0.03
✓ ✗ ✓	MAE (S)MAPE(%) RMSE	0.2081 \pm 0.00 49.938 \pm 0.72 0.2899 \pm 0.00	0.1796 \pm 0.01 36.296 \pm 1.02 0.2525 \pm 0.01	0.2135 \pm 0.01 19.150 \pm 0.82 0.2693 \pm 0.01	0.1025 \pm 0.01 14.070 \pm 0.44 0.1367 \pm 0.01	0.1325 \pm 0.01 10.228 \pm 0.27 0.1921 \pm 0.01
✗ ✓ ✓	MAE (S)MAPE(%) RMSE	0.1662 \pm 0.01 43.518 \pm 2.72 0.2609 \pm 0.01	0.1138 \pm 0.01 28.090 \pm 1.96 0.2132 \pm 0.01	0.2691 \pm 0.01 28.484 \pm 0.90 0.4574 \pm 0.02	0.1737 \pm 0.04 22.438 \pm 3.39 0.2799 \pm 0.06	0.1130 \pm 0.01 9.608 \pm 0.30 0.2431 \pm 0.01
✓ ✗ ✗	MAE (S)MAPE(%) RMSE	0.2059 \pm 0.00 50.194 \pm 0.84 0.2900 \pm 0.00	0.1647 \pm 0.01 34.990 \pm 1.27 0.2419 \pm 0.01	0.2420 \pm 0.07 21.634 \pm 2.35 0.3330 \pm 0.07	0.1829 \pm 0.03 19.832 \pm 4.82 0.2589 \pm 0.03	0.1737 \pm 0.03 11.826 \pm 1.34 0.2541 \pm 0.04
✗ ✓ ✗	MAE (S)MAPE(%) RMSE	0.1931 \pm 0.00 49.064 \pm 0.97 0.2859 \pm 0.01	0.1451 \pm 0.00 33.790 \pm 0.44 0.2383 \pm 0.00	0.3338 \pm 0.05 30.714 \pm 3.11 0.5526 \pm 0.11	0.2198 \pm 0.05 19.882 \pm 2.03 0.3144 \pm 0.06	0.1428 \pm 0.03 10.408 \pm 0.92 0.2884 \pm 0.05
✗ ✗ ✓	MAE (S)MAPE(%) RMSE	0.1969 \pm 0.00 50.042 \pm 0.46 0.2865 \pm 0.00	0.1594 \pm 0.00 35.146 \pm 0.38 0.2414 \pm 0.00	0.2805 \pm 0.05 28.466 \pm 4.56 0.4358 \pm 0.08	0.1533 \pm 0.10 17.072 \pm 4.35 0.2501 \pm 0.13	0.1170 \pm 0.02 9.690 \pm 0.70 0.2429 \pm 0.02
✗ ✗ ✗	MAE (S)MAPE(%) RMSE	0.2055 \pm 0.00 50.774 \pm 0.55 0.2919 \pm 0.00	0.1654 \pm 0.00 35.880 \pm 0.39 0.2466 \pm 0.00	0.5510 \pm 0.19 35.366 \pm 4.46 0.9542 \pm 0.37	0.2750 \pm 0.14 22.500 \pm 3.80 0.4336 \pm 0.23	0.1724 \pm 0.12 10.986 \pm 3.25 0.3458 \pm 0.22

prediction methods based on pre-trained models should consider the nature of the multivariate context. When variable count is low and multivariate information is less critical, a combination of cross-domain pre-trained backbones and zero-initialized regression suffices. Our meta-variable low rank multivariate fusion method is nonetheless applicable to most practical scenarios where multivariate modeling is essential.

3. **Zero initialization:** Zero initialization provides a simple yet effective strategy for stabilizing training in pre-trained RUL prediction models. Models with zero-initialized regressors exhibit significantly lower variance across multiple runs, especially for MAPE and SMAPE metrics. Notably, even without backbone pre-training, the zero-initialized regressor greatly reduces prediction errors and can serve as a general-purpose regression head.

4.4.3. Fine-tuning Stability

To further validate the effectiveness of zero initialization and its impact on the optimization process, we conduct stability experiments. We compare 3 configurations: ResNet-18 pre-trained with FEI (marked as **Pre-trained**), ResNet-18 with the full PEFT-MuTS architecture (marked as **PEFT-MuTS**), and randomly initialized ResNet-18 (marked as **Random Init.**).

We fix a set of evaluation samples that are excluded from the gradient update process and record the standard deviation(std) of their backbone output feature's ℓ_2 norm across batches, denoted as $\sigma||z||_2$. A larger variance indicates a more unstable training process, which is also reflected in the variance of the training loss curves. We visualize the training process on the FD002-1 dataset, as shown in Figure 4. This includes both the training loss variance curves and the $\sigma||z||_2$ trajectories for the evaluation samples.

In the figure, green curves represent results using Kaiming-initialized regressors, while purple curves correspond to zero-initialized ones. Shaded regions show the standard deviation across multiple runs. We observe the following:

All models exhibit an initial fluctuation phase (first 10 epochs), during which the feature std $\sigma||z||_2$ first increases then stabilizes. High early std leads to greater divergence among runs, which is particularly pronounced in the PEFT-MuTS loss curves—consistent with the theoretical analysis in Section 3.3. After applying zero initialization (purple

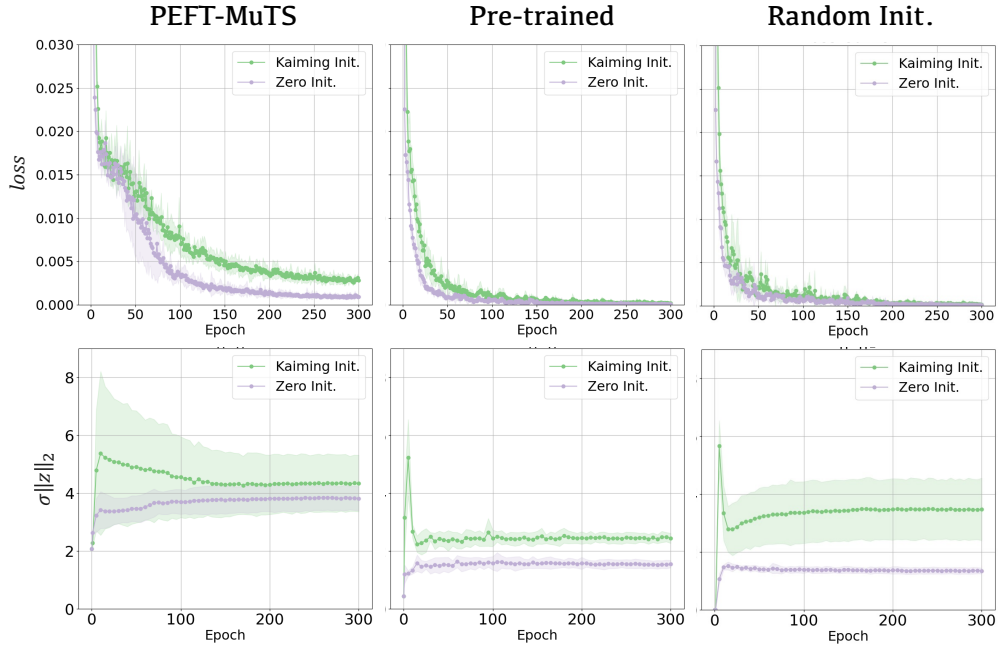


Figure 4: Evolution of training loss and the std of feature ℓ_2 norms over training epochs.

curves), the variance from (14) is suppressed. The std of the feature norm stabilizes more quickly, reducing loss value and accelerating convergence toward lower loss values in PEFT-MuTS. The positive effect of zero initialization is more prominent for pre-trained models (PEFT-MuTS, Pre-trained) than for randomly initialized ones. This is because pre-training yields high initial feature variance, while random initialization naturally leads to low variance, again aligning with the theoretical analysis.

Combined with the ablation results in Table 5, we conclude that the zero-initialized regressor greatly enhances convergence speed and generalization when used in pre-trained-based RUL prediction models.

4.4.4. Hyperparameter Sensitivity

In Side Tuning-based PEFT methods, the projected dimension r_k (i.e., of \mathbf{A}_k and \mathbf{B}_k in (3)) is a key hyperparameter. Contrary to the convention in CV and NLP that favors extremely low r_k values[22, 25], our experiments show that allocating larger r_k to shallow layers and smaller r_k to deeper ones yields better performance under a fixed parameter budget (see Figure 5).

The horizontal axis in Figure 5 shows different layer-wise r_k settings (e.g., [256, 64, 64, 4, 4, 2, 2, 1] from shallow to deep). Increasing r_k in early layers consistently reduces test error. However, excessively large r_k can inflate parameter count—for example, 88.5K in the first configuration vs. 52.9K in the second—potentially leading to overfitting.

Given that ResNet-18 generates high-dimensional features in deeper layers, using large r_k there would cause exponential parameter growth. To balance efficiency and effectiveness, we adopt smaller r_k values in deeper layers, aligning with standard practices in PEFT[23][24][25].

5. Conclusion and Future Work

This paper proposes PEFT-MuTS, the first framework to integrate cross-domain representation learning with PEFT for few-shot RUL prediction. By leveraging cross-domain pre-training, PEFT-MuTS reduces reliance on scarce in-domain data and generalizes well with minimal degradation samples. The proposed PEFT-MuTS framework successfully adapts univariate pretrained backbone networks to multivariate RUL prediction tasks through the Independent Feature Tuning Network and Meta-Variable-based Low-Rank Feature Fusion. By leveraging a simple yet effective zero-initialized regressor, it significantly improves fine-tuning stability when applying pretrained models. On the C-MAPSS and XJTU-SY Bearing datasets, PEFT-MuTS substantially outperforms existing few-shot RUL

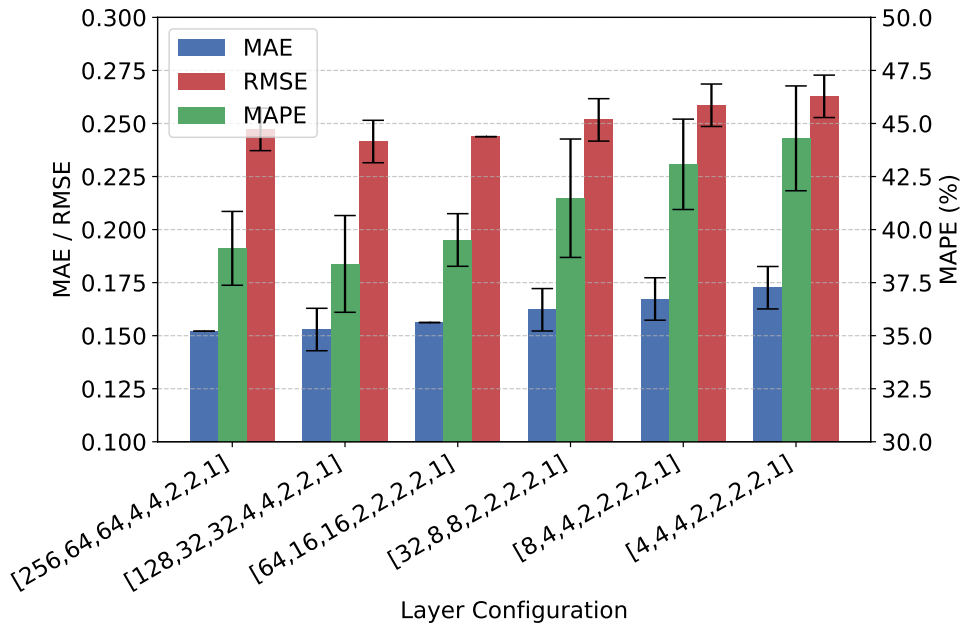


Figure 5: Performance under different projected dimensions r on the FD002-1 dataset.

prediction methods using less than 1% of the available data, demonstrating the effectiveness of cross-domain temporal knowledge transfer for RUL prediction. This framework extends the transfer perspective from “identifying similar degradation patterns” to “leveraging generalizable temporal priors,” offering a new paradigm for few-shot RUL prediction research.

Potential directions for future research include:

1. Source-domain transferability: Investigating how to quantify the transferability of source-domain data to target-domain degradation sequences, thereby enhancing the interpretability of general temporal knowledge for degradation time series.
2. Hybrid sample utilization: Combining cross-domain samples with domain-specific samples from similar equipment to improve few-shot prediction accuracy when data from similar devices are available.

CRediT authorship contribution statement

En Fu: Methodology, Software, Writing. **Yanyan Hu:** Methodology, Revision. **Changhua Hu:** Validation, Revision. **Zengwang Jin:** Revision. **Kaixiang Peng:** Revision.

References

[1] Renpeng Mo, Han Zhou, Hongpeng Yin, and Xiaosheng Si. A survey on few-shot learning for remaining useful life prediction. *Reliability Engineering & System Safety*, page 110850, 2025.

[2] Jianghong Zhou and Yi Qin. A continuous remaining useful life prediction method with multistage attention convolutional neural network and knowledge weight constraint. *IEEE Transactions on Neural Networks and Learning Systems*, 2024.

[3] Wenda Kang, Dianpeng Wang, Geurt Jongbloed, Jiawen Hu, and Piao Chen. Robust transfer learning for battery lifetime prediction using early cycle data. *IEEE Transactions on Industrial Informatics*, 2025.

[4] Junhao Chen, Chunhui Zhao, and Jinliang Ding. A flexible probabilistic framework with concurrent analysis of continuous and categorical data for industrial fault detection and diagnosis. *IEEE Transactions on Industrial Informatics*, 19(10):10578–10590, 2023.

[5] Yuru Zhang, Chun Su, Xiaoliang He, Mingjiang Xie, Zhigang Tian, and Hao Liu. Multi-source domain generalization for machine remaining useful life prediction via risk minimization-based test-time adaptation. *IEEE Transactions on Industrial Informatics*, 2024.

[6] Lingli Cui, Yongchang Xiao, Dongdong Liu, and Honggui Han. Digital twin-driven graph domain adaptation neural network for remaining useful life prediction of rolling bearing. *Reliability Engineering & System Safety*, 245:109991, 2024.

[7] Yifei Ding, Peng Ding, Xiaoli Zhao, Yudong Cao, and Minping Jia. Transfer learning for remaining useful life prediction across operating conditions based on multisource domain adaptation. *IEEE/ASME transactions on mechatronics*, 27(5):4143–4152, 2022.

[8] Haodong Li, Peng Cao, Xingwei Wang, Ying Li, Bo Yi, and Min Huang. Pre-training enhanced unsupervised contrastive domain adaptation for industrial equipment remaining useful life prediction. *Advanced Engineering Informatics*, 60:102517, 2024.

[9] Mohamed Ragab, Zhenghua Chen, Min Wu, Chuan Sheng Foo, Chee Keong Kwoh, Ruqiang Yan, and Xiaoli Li. Contrastive adversarial domain adaptation for machine remaining useful life prediction. *IEEE Transactions on Industrial Informatics*, 17(8):5239–5249, 2020.

[10] Jie Shang, Danyang Xu, Mingyu Li, Haobo Qiu, Chen Jiang, and Liang Gao. Remaining useful life prediction of rotating equipment under multiple operating conditions via multi-source adversarial distillation domain adaptation. *Reliability Engineering & System Safety*, 256:110769, 2025.

[11] Kangkai Wu, Jingjing Li, Lin Zuo, Ke Lu, and Heng Tao Shen. Weighted adversarial domain adaptation for machine remaining useful life prediction. *IEEE Transactions on Instrumentation and Measurement*, 71:1–11, 2022.

[12] Jakob Schmitt, Ivo Horstötter, and Bernard Bäker. Effective estimation of battery state-of-health by virtual experiments via transfer-and meta-learning. *Journal of Energy Storage*, 63:106969, 2023.

[13] Lixiao Cao, Xueping Wang, Hongyu Zhang, Zong Meng, Jimeng Li, and Miaoqiao Liu. A novel cross-scenario transferable rul prediction network with multisource domain meta transfer learning for wind turbine bearings. *IEEE Transactions on Instrumentation and Measurement*, 2025.

[14] Liang Chang and Yan-Hui Lin. Few-shot remaining useful life prediction based on bayesian meta-learning with predictive uncertainty calibration. *Engineering Applications of Artificial Intelligence*, 142:109980, 2025.

[15] Daoming She, Yudan Duan, Zhichao Yang, and Michael Pecht. A meta-transfer learning prediction method with few-shot data for the remaining useful life of rolling bearing. *Structural Health Monitoring*, page 14759217251321080, 2025.

[16] Peng Ding, Minping Jia, Yifei Ding, Yudong Cao, and Xiaoli Zhao. Intelligent machinery health prognostics under variable operation conditions with limited and variable-length data. *Advanced Engineering Informatics*, 53:101691, 2022.

[17] Jichao Zhuang, Minping Jia, Cheng-Geng Huang, Michael Beer, and Ke Feng. Health prognosis of bearings based on transferable autoregressive recurrent adaptation with few-shot learning. *Mechanical Systems and Signal Processing*, 211:111186, 2024.

[18] Jiaxiang Dong, Haixu Wu, Haoran Zhang, Li Zhang, Jianmin Wang, and Mingsheng Long. Simmtm: A simple pre-training framework for masked time-series modeling. *Advances in Neural Information Processing Systems*, 36:29996–30025, 2023.

[19] Xiang Zhang, Ziyuan Zhao, Theodoros Tsiligkaridis, and Marinka Zitnik. Self-supervised contrastive pre-training for time series via time-frequency consistency. *Advances in neural information processing systems*, 35:3988–4003, 2022.

[20] En Fu and Yanyan Hu. Frequency-masked embedding inference: A non-contrastive approach for time series representation learning. In *Proceedings of the AAAI Conference on Artificial Intelligence*, volume 39, pages 16639–16647, 2025.

[21] Zhihan Yue, Yujing Wang, Juanyong Duan, Tianmeng Yang, Congrui Huang, Yunhai Tong, and Bixiong Xu. Ts2vec: Towards universal representation of time series. In *Proceedings of the AAAI conference on artificial intelligence*, volume 36, pages 8980–8987, 2022.

[22] Yi Xin, Siqi Luo, Haodi Zhou, Junlong Du, Xiaohong Liu, Yue Fan, Qing Li, and Yuntao Du. Parameter-efficient fine-tuning for pre-trained vision models: A survey. *arXiv e-prints*, pages arXiv–2402, 2024.

[23] Jeffrey O Zhang, Alexander Sax, Amir Zamir, Leonidas Guibas, and Jitendra Malik. Side-tuning: a baseline for network adaptation via additive side networks. In *European conference on computer vision*, pages 698–714. Springer, 2020.

[24] René Ranftl, Alexey Bochkovskiy, and Vladlen Koltun. Vision transformers for dense prediction. In *Proceedings of the IEEE/CVF international conference on computer vision*, pages 12179–12188, 2021.

[25] Minghao Fu, Ke Zhu, and Jianxin Wu. Dtl: Disentangled transfer learning for visual recognition. In *Proceedings of the AAAI conference on artificial intelligence*, volume 38, pages 12082–12090, 2024.

[26] Md Kowsher, Nusrat Jahan Pratasha, and Prakash Bhat. Propulsion: Steering llm with tiny fine-tuning. In *Proceedings of the 31st International Conference on Computational Linguistics*, pages 7569–7597, 2025.

[27] Xiao Liu, Kaixuan Ji, Yicheng Fu, Weng Tam, Zhengxiao Du, Zhilin Yang, and Jie Tang. P-tuning: Prompt tuning can be comparable to fine-tuning across scales and tasks. In *Proceedings of the 60th Annual Meeting of the Association for Computational Linguistics (Volume 2: Short Papers)*, pages 103–108, 2022.

Short Papers), pages 61–68, 2022.

- [28] Beier Zhu, Yulei Niu, Yucheng Han, Yue Wu, and Hanwang Zhang. Prompt-aligned gradient for prompt tuning. In *Proceedings of the IEEE/CVF international conference on computer vision*, pages 15659–15669, 2023.
- [29] Edward J Hu, Yelong Shen, Phillip Wallis, Zeyuan Allen-Zhu, Yuanzhi Li, Shean Wang, Lu Wang, Weizhu Chen, et al. Lora: Low-rank adaptation of large language models. *ICLR*, 1(2):3, 2022.
- [30] Yu Yu, Chao-Han Huck Yang, Jari Kolehmainen, Prashanth G Shivakumar, Yile Gu, Sungho Ryu Roger Ren, Qi Luo, Aditya Gourav, I-Fan Chen, Yi-Chieh Liu, et al. Low-rank adaptation of large language model rescoring for parameter-efficient speech recognition. In *2023 IEEE Automatic Speech Recognition and Understanding Workshop (ASRU)*, pages 1–8. IEEE, 2023.
- [31] En Fu, Yanyan Hu, Kaixiang Peng, and Yuxin Chu. Supervised contrastive learning based dual-mixer model for remaining useful life prediction. *Reliability Engineering & System Safety*, 251:110398, 2024.
- [32] Jiusi Zhang, Xiang Li, Jilun Tian, Hao Luo, and Shen Yin. An integrated multi-head dual sparse self-attention network for remaining useful life prediction. *Reliability Engineering & System Safety*, 233:109096, 2023.
- [33] Stefan Elfwing, Eiji Uchibe, and Kenji Doya. Sigmoid-weighted linear units for neural network function approximation in reinforcement learning. *Neural networks*, 107:3–11, 2018.
- [34] Xavier Glorot and Yoshua Bengio. Understanding the difficulty of training deep feedforward neural networks. In *Proceedings of the thirteenth international conference on artificial intelligence and statistics*, pages 249–256. JMLR Workshop and Conference Proceedings, 2010.
- [35] Kaiming He, Xiangyu Zhang, Shaoqing Ren, and Jian Sun. Delving deep into rectifiers: Surpassing human-level performance on imagenet classification. In *Proceedings of the IEEE international conference on computer vision*, pages 1026–1034, 2015.
- [36] Abhinav Saxena, Kai Goebel, Don Simon, and Neil Eklund. Damage propagation modeling for aircraft engine run-to-failure simulation. In *2008 international conference on prognostics and health management*, pages 1–9. IEEE, 2008.
- [37] Biao Wang, Yaguo Lei, Naipeng Li, and Ningbo Li. A hybrid prognostics approach for estimating remaining useful life of rolling element bearings. *IEEE Transactions on Reliability*, 69(1):401–412, 2018.
- [38] Fei Jiang, Kang Ding, Guolin He, Huibin Lin, Zhuyun Chen, and Weihua Li. Dual-attention-based multiscale convolutional neural network with stage division for remaining useful life prediction of rolling bearings. *IEEE Transactions on Instrumentation and Measurement*, 71:1–10, 2022.
- [39] Xuanyuan Su, Hongmei Liu, Laifa Tao, Chen Lu, and Mingliang Suo. An end-to-end framework for remaining useful life prediction of rolling bearing based on feature pre-extraction mechanism and deep adaptive transformer model. *Computers & Industrial Engineering*, 161:107531, 2021.
- [40] Bob Kemp, Aeilko H Zwinderman, Bert Tuk, Hilbert AC Kamphuisen, and Josefien JL Oberye. Analysis of a sleep-dependent neuronal feedback loop: the slow-wave microcontinuity of the eeg. *IEEE Transactions on Biomedical Engineering*, 47(9):1185–1194, 2000.
- [41] Yu Wang, Shujie Liu, Shuai Lv, and Gengshuo Liu. Meta-learning and knowledge discovery based physics-informed neural network for remaining useful life prediction. *arXiv preprint arXiv:2504.13797*, 2025.
- [42] Yubo Hou, Mohamed Ragab, Min Wu, Chee-Keong Kwoh, Xiaoli Li, and Zhenghua Chen. Target-specific adaptation and consistent degradation alignment for cross-domain remaining useful life prediction. *IEEE Transactions on Automation Science and Engineering*, 2025.
- [43] Wensi Tang, Guodong Long, Lu Liu, Tianyi Zhou, Jing Jiang, and Michael Blumenstein. Rethinking 1d-cnn for time series classification: A stronger baseline. *arXiv preprint arXiv:2002.10061*, pages 1–7, 2020.